Effect of Particle Size of $FePO_4 \cdot 2H_2O$ on the Physical and Electrochemical Properties of $LiFePO_4$/C Cathode for LIBs

Guangwei Geng[1], Yuanchao Li[2,*], Xiaokun Shang[3], Baoyan Xing[2], Kaiyang Zhou[2], Zhaoting Shang[2], Li Yang[2], Guangri Xu[2] and Jinghao Hao[1,*]

[1] Faculty of Science, Henan University of Animal Husbandry and Economics, Zhengzhou 450046, P. R. China
[2] School of Chemistry and Chemical Engineering, Henan Institute of Science and Technology, Xinxiang, 453003, P. R. China
[3] The Battery Research Institute of HeNan, Xinxiang, 453003, P. R. China
[*]E-mail: liyuanchaozzu@126.com (Y.C. Li), haojinghao2021@126.com (J.H. Hao)

Particle size is a very important factor for the electrochemical performance of materials. However, the effect of the particle size of $FePO_4 \cdot 2H_2O$ on the properties of $LiFePO_4$ remains unclear during carbon thermal reduction using $FePO_4 \cdot 2H_2O$ as a raw material. Here, $LiFePO_4$/C composites are synthesized by an aqueous rheological phase-assisted carbon thermal reduction method using $FePO_4 \cdot 2H_2O$ with different particle sizes as raw materials. The particle size of $LiFePO_4$ is positively correlated with the particle size of $FePO_4 \cdot 2H_2O$. The $LiFePO_4$ materials prepared using small-sized $FePO_4 \cdot 2H_2O$ show high purity and small particle size, thus exhibiting an improved rate capacity of 160 mA h g^{-1} at 0.1 C and 135 mA h g^{-1} at 5 C and cycling stability with a capacity retention of 98.9% after 100 cycles at 2 C. Intriguingly, the LiFePO4 materials prepared using large-sized $FePO_4$ show a longer slope voltage at the end of the discharge curve, which could be accounted for by an Fe^{3+} phase on the surface of the large-sized $LiFePO_4$. Our studies provide a new understanding of the effect of the particle size of $FePO_4 \cdot 2H_2O$ on the properties of $LiFePO_4$ materials during carbon thermal reduction.

1. INTRODUCTION

Lithium-ion batteries have attracted attention as power sources for electric vehicles and hybrid electric vehicles. However, the safety, cost and power performance of lithium-ion batteries are key issues limiting their application in electric vehicles [1,2]. These indices of lithium-ion batteries are mainly restricted by the performance of cathode materials. Therefore, finding a suitable cathode material has become the main task of lithium-ion batteries applied to electric vehicles. Among the developed cathode materials, $LiFePO_4$ is considered the most promising cathode material for lithium-ion batteries due to its

low raw material cost, high safety and environmental friendliness. However, the low electronic conductivity and slow Li ion diffusion limit its electrochemical performance, especially its power capacity [3,4]. The strategy of improving the electronic conductivity and Li-ion diffusion mainly includes coating with conductive carbon [5-8], doping with metal ions [9-12] and reducing the particle size [13-17]. Among them, the electronic conductivity is mainly increased by coating with conductive carbon and doping with metal ions; the Li ion diffusion is mainly increased by reducing the particle size. Generally, the shortened diffusion distance of Li ions makes nanoparticle-sized $LiFePO_4$ have a better rate performance than large particle-sized $LiFePO_4$ [18-22]. For lithium ions or electrons, large particles not only increase the diffusion path but also block the diffusion of lithium ions easily, which greatly limits the electrochemical performance of $LiFePO_4$ materials.

Although reducing the particle size is particularly effective for improving the Li ion diffusion of $LiFePO_4$, some issues related to reducing the particle size still remain unclear, including defect chemistry associated with $LiFePO_4$ nanoparticles [23-25]; the effect of particle size on single-phase versus two-phase insertion processes [26-28]; the formation of secondary phases [29,30]; and the effect of $LiFePO_4$ particle size on the surface/interface reactions [30-33]. Gibot [26] synthesized $LiFePO_4$ with different particle sizes, in which $LiFePO_4$ with a particle size of 40 nm had a sloping curve at the end of discharge compared with $LiFePO_4$ with other particle sizes. Such a sloping curve was considered to be a single-phase electrochemical behaviour, so changing the particle size can make the Li insertion/deinsertion mechanism of $LiFePO_4$ shift from a two-phase process to a single-phase process. Unlike Gibot's report that the sloping curve is caused by the decrease in the particle size of $LiFePO_4$, Kang [27] also prepared such a $LiFePO_4$ material with a sloping curve at the end of discharge through controlled off-stoichiometry. The sloping curve was considered to indicate the presence of a fast ion-conducting ferric phase containing $Li_4P_2O_7$, which possesses electrical activity with a low discharge voltage plateau. Therefore, the origin of this sloping curve at the end of discharge is still not clear, and further research is needed.

In this paper, $LiFePO_4$ materials were synthesized by a rheological phase-assisted carbon thermal reduction method using $FePO_4 \cdot 2H_2O$ with different particle sizes as raw materials. The effects of particle sizes of $FePO_4 \cdot 2H_2O$ on the electrochemical properties of the as-synthesized $LiFePO_4$ materials were investigated. The $LiFePO_4/C$ materials prepared using small-sized $FePO_4 \cdot 2H_2O$ exhibited superior electrochemical performances due to the improved purity and reduced particle sizes of the as-synthesized $LiFePO_4/C$ materials. The $LiFePO_4/C$ materials prepared using large-sized $FePO_4 \cdot 2H_2O$ exhibited a longer slope voltage at the end of the discharge curve due to the electrically active Fe^{3+} phase formed on the surface of the $LiFePO_4/C$ materials.

2. EXPERIMENTAL SECTION

2.1. Synthesis procedure

$FePO_4 \cdot 2H_2O$ raw materials with different particle sizes were prepared by adjusting the concentration of H_3PO_4 via a modified method as previously reported [34]. $LiFePO_4/C$ was prepared via a rheological phase-assisted carbon thermal reduction method from $FePO_4 \cdot 2H_2O$ raw materials. Under

stirring, $LiOH \cdot H_2O$ (103 *at.%*) and sucrose (14.3 *wt.%*) were completely dissolved in distilled water (173 *wt.%*), and the pH of the aforementioned solution was adjusted to 9 with acetic acid to guarantee that all of the raw materials dissolved. Then, to produce a suspension slurry, the as-prepared $FePO_4 \cdot 2H_2O$ (100 *at.%*) was added to the solution. The suspension slurry was heated at 70 °C under continuous stirring to obtain a homogeneous rheological body before drying at 110 °C to evaporate the residual water. The formed precursor was finally ball milled for 3 h and calcined for 10 h at 700 °C in a N_2 atmosphere to obtain a black powder of $LiFePO_4$. The $LiFePO_4$/C samples prepared using $FePO_4 \cdot 2H_2O$ raw materials with 1, 2, and 5 μm particle sizes were designated S-LFP, M-LFP, and L-LFP, respectively.

2.2. Material characterization

The X-ray powder diffraction patterns were recorded on an X'pert PRO Panalytical diffractometer with Cu Kα radiation (λ=1.54178 Å) with a step size of 0.017. The micromorphology of $LiFePO_4$ powders was observed using a JSM-6360LV scanning electron microscope (SEM). TEM images were characterized by a high resolution transmission electron microscope (JEM 2100). X-ray photoelectron spectra (XPS) were recorded on a PHI Quantera SXM spectrometer with an Al Kα = 280.00 eV excitation source, where the binding energies were referenced to the C1s line at 284.8 eV from adventitious carbon.

2.3. Electrochemical measurements

The positive electrodes were prepared by coating aluminum foil with a slurry composed of 80% $LiFePO_4$, 10% polyvinylidene (PVDF) binder and 10% mixed additives of KS6 and Super-P (1:1 *wt.%*) in N-methyl-2-pyrrolidone. The electrodes were then dried at 110 °C under vacuum for 12 h. Then the electrodes were pressed under a proper pressure and punched in the form of 14 mm diameter disks. The loading density of the electrode was about 3 mg cm^{-2}. Based on the mass of the $LiFePO_4$/C materials in the electrode, Current densities and specific capacities were calculated. Current densities and specific capacities were calculated on basis of the loading mass of the electroactive materials. Lithium metal served as the anode and a 1 M solution of $LiPF_6$ was used as the electrolyte(w/w 1:1 ethylene carbonate: dimethyl carbonate). CR2016 coin cells were fabricated in an Ar-filled glove box. Galvanostatic cycling measurements of the above-prepared cells were conducted on a LAND battery program-control test system (Wuhan, China) in 2.0−4.2 V. Electrochemical impedance spectroscopy (EIS) were conducted on a CHI660C electrochemical analyzer (Shanghai Chenhua). Electrochemical impedance spectra were recorded under an ac perturbation signal of 5 mV over a frequency range of 100 kHz to 10 mHz.

Int. J. Electrochem. Sci., 17 **(2022)** Article Number: 220722

4

3. RESULTS AND DISCUSSION
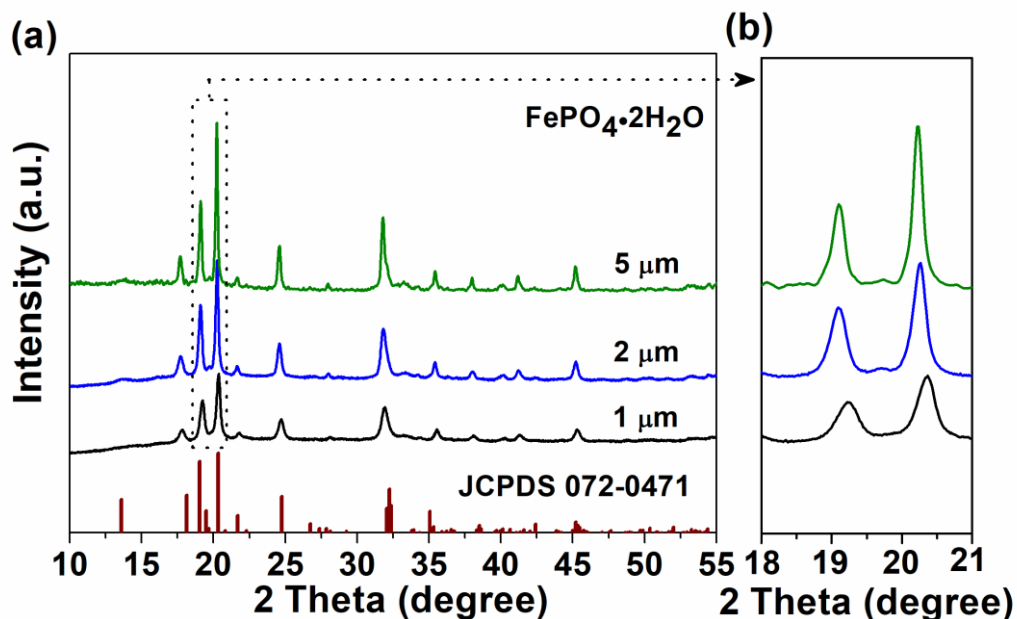
Figure 1. XRD patterns (a) and peak magnification (b) of $FePO_4 \cdot 2H_2O$ raw materials with different particle sizes.
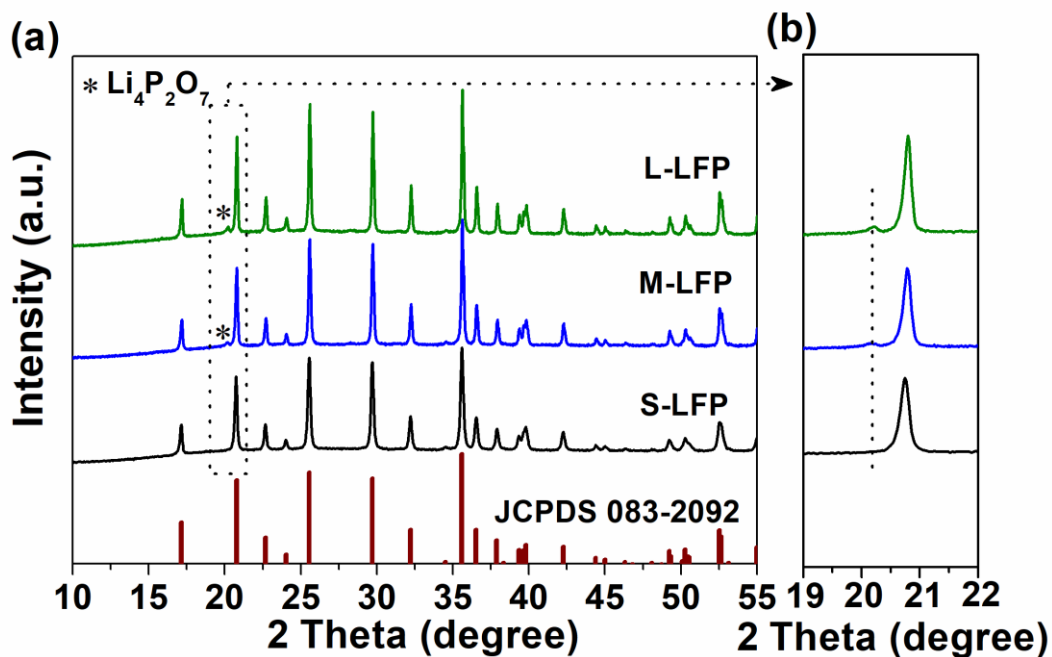
Figure 2. XRD patterns (a) and peak magnification (b) of $LiFePO_4$ prepared using $FePO_4 \cdot 2H_2O$ with different particle sizes as raw materials.

Figure 1 shows the XRD patterns of the $FePO_4 \cdot 2H_2O$ raw materials with different particle sizes. In Figure 1, the diffraction peaks of the $FePO_4 \cdot 2H_2O$ raw materials with different particle sizes are well

matched with those of monoclinic $FePO_4 \cdot 2H_2O$ (01-072-0471), except for the diffraction peak at $2\theta=13.5°$ (011). The diffraction peaks of $FePO_4 \cdot 2H_2O$ with a small particle size (1 μm) are shifted towards larger angles. The peak intensities of the as-prepared $FePO_4 \cdot 2H_2O$ raw materials intensified as the $FePO_4 \cdot 2H_2O$ particle size increased.
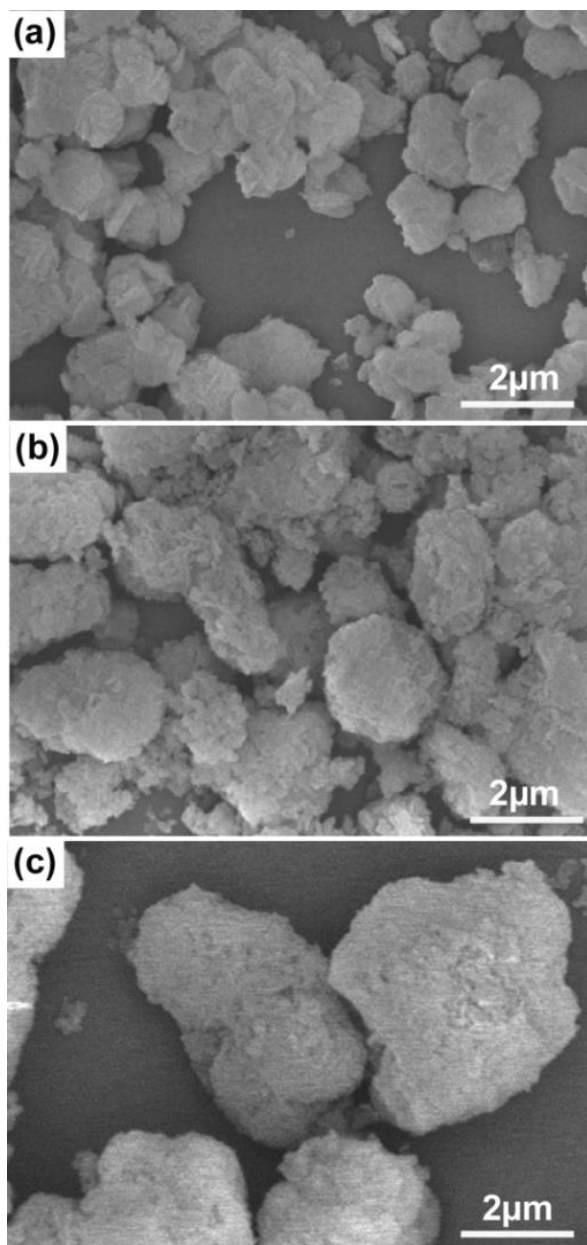
Figure 3. SEM images of $FePO_4 \cdot 2H_2O$ raw materials with different particle sizes: 1 μm $FePO_4 \cdot 2H_2O$ (a), 2 μm $FePO_4 \cdot 2H_2O$ (b) and 5 μm $FePO_4 \cdot 2H_2O$ (c).

This result demonstrates a correlation between the diffraction peak intensity and particle size of $FePO_4 \cdot 2H_2O$. Figure 2 shows XRD patterns of LFP/C samples prepared using different particle sizes. It is seen that the S-LFP sample shows a pure LFP phase with no additional diffraction peak, while for the M-LFP and L-LFP samples with larger particles, the diffraction peak of a $Li_4P_2O_7$ impure phase appears. This indicates that large $FePO_4 \cdot 2H_2O$ leads to the formation of the impure phase. It is worth noting that

different crystal structures, morphologies and purities of $FePO_4 \cdot 2H_2O$ have an effect on the final $LiFePO_4$ samples [35].

The SEM images of $FePO_4 \cdot 2H_2O$ raw materials with different particle sizes are shown in Figure 3. The as-prepared $FePO_4 \cdot 2H_2O$ raw materials have a near-spherical morphology and different particle sizes. The particle sizes of the as-prepared $FePO_4 \cdot 2H_2O$ are approximately 1 μm, 2 μm and 5 μm, respectively. SEM images of the LFP samples prepared with different sizes of $FePO_4 \cdot 2H_2O$ are shown in Figure 4. The S-LFP sample shows a uniform morphology and particle distribution. In the M-LFP sample prepared using larger $FePO_4 \cdot 2H_2O$ particles, some large agglomerated LFP particles appear. With the increase in the particle size of $FePO_4 \cdot 2H_2O$, some larger agglomerated LFP particles with a flat elliptical morphology emerge in the L-LFP sample. These results indicate that the particle size of the LFP samples prepared using $FePO_4 \cdot 2H_2O$ as raw materials inherited the particle size of the $FePO_4 \cdot 2H_2O$ raw materials. The HRTEM image of the S-LFP sample in Figure 3d indicates that there is a carbon layer ~3 nm thick on the surface of the LFP materials.
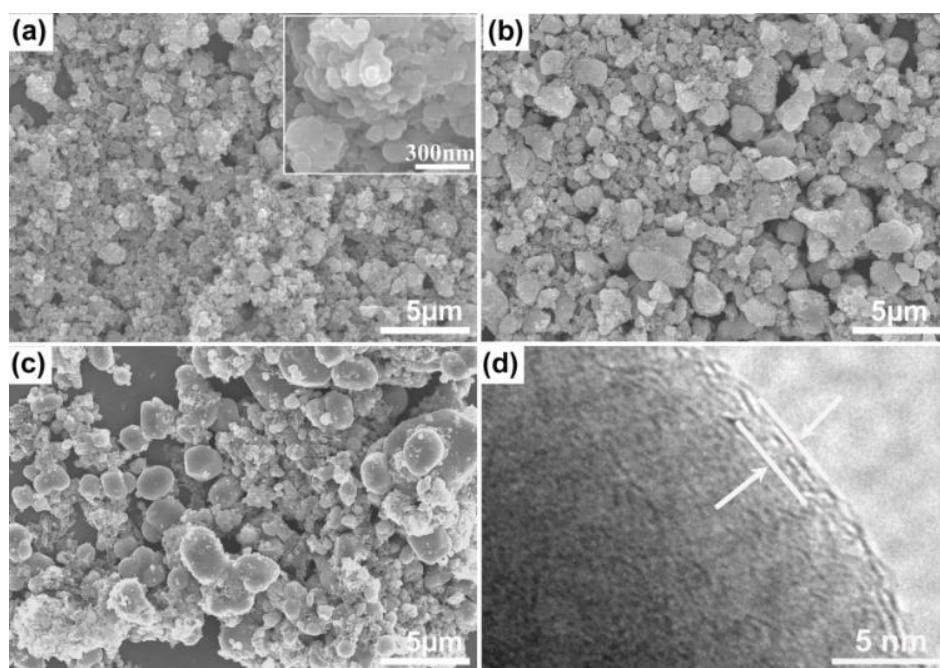
Figure 4. SEM images of the S-LFP (a), M-LFP (b) and L-LFP (c) samples and HRTEM image (d) of the S-LFP sample.

The electrochemical performances of the as-prepared LFP/C samples are shown in Figure 5. The charge–discharge curves in Figure 4a show discharge capacities of 160, 158, and 145 mAh g^{-1} at 0.1 C for the S-LFP, M-LFP and L-LFP samples, indicating that the initial capacity of the as-prepared LFP samples decreases with increasing particle size of the $FePO_4 \cdot 2H_2O$ raw materials. Combined with the XRD and SEM data, the decreased capacity of LFP samples with large particle sizes can be attributed to the formation of an impure phase and large LFP particles caused by large $FePO_4 \cdot 2H_2O$ particles. In addition, the M-LFP and L-LFP samples with large particle sizes show longer slope curves at the end of

discharge, which could be released by the unreacted $FePO_4$ phase inside the large $FePO_4 \cdot 2H_2O$ particles [30]. Based on the above results, we speculate that large $FePO_4 \cdot 2H_2O$ particles give rise to no lithiation of the $FePO_4$ core, resulting in excess Li on the surface of LFP materials and forming an impure phase in the LFP materials.
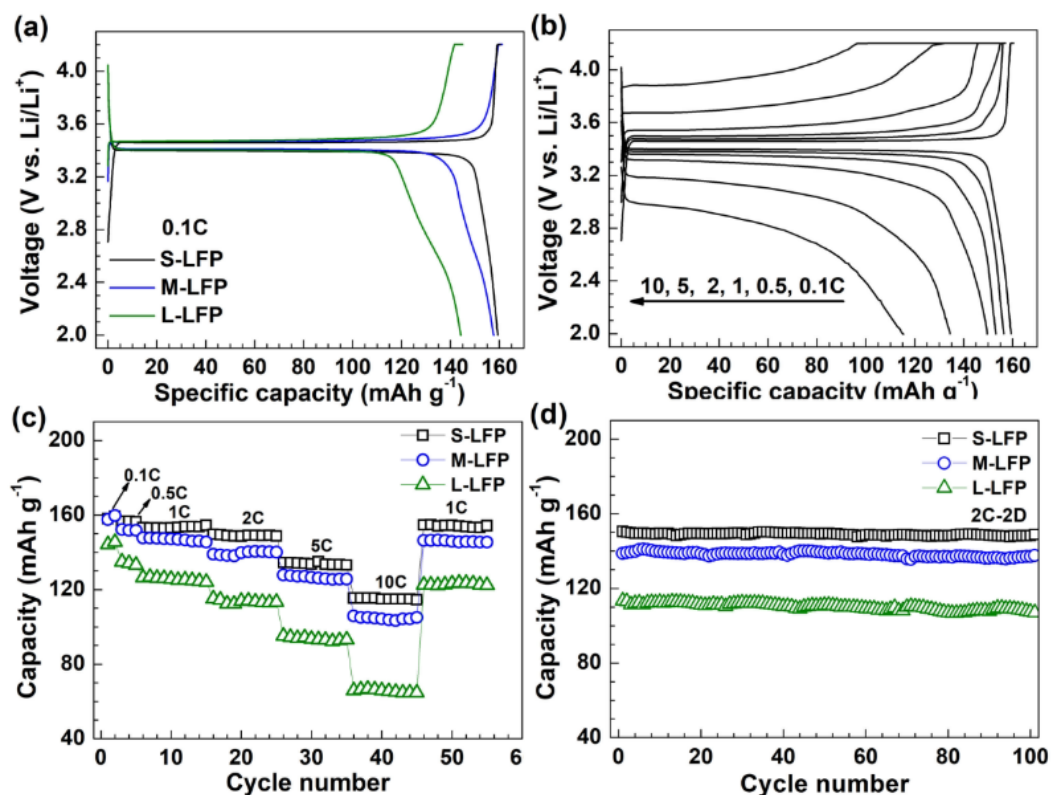

Figure 5. Initial charge/discharge curves (a), rate capability (c) and recyclability (d) of the S-LFP, M-LFP and L-LFP samples and charge/discharge curves (b) of the S-LFP sample at various rates.

Figure 5b presents the voltage-capacity curves of S-LFP at different rates. S-LFP exhibits discharge plateaus of 3.34, 3.27, and 3.10 V at high rates of 1, 2, and 5 C, respectively, demonstrating the fast intercalation/deintercalation behaviour of Li ions in bulk LFP [36]. The S-LFP sample delivers discharge capacities of 159, 156, 153, 149, 134, and 115 mA h g^{-1} at 0.1, 0.5, 1, 2, 5, and 10 C, respectively, which are higher than those of M-LFP and L-LFP samples (Figure 5c). This result demonstrates that the use of $FePO_4 \cdot 2H_2O$ raw materials with small particles contributes to the high purity and reduced particle size of LFP materials, thus leading to the superior rate performance of the S-LFP sample.

The cycling performance of the as-prepared samples is displayed in Figure 5d. S-LFP exhibits the best stability with a discharge capacity of approximately 149 mA h g^{-1} at 2 C after 100 cycles, corresponding to a capacity retention of 98.9%. For the M-LFP and L-LFP samples, the discharge capacity after 100 cycles at 2 C is approximately 137 and 107 mA h g^{-1} with capacity retentions of 97.6%

and 94.5%, respectively. This further confirms the positive effect of the high purity and reduced particle size on the electrochemical performance of LFP materials.
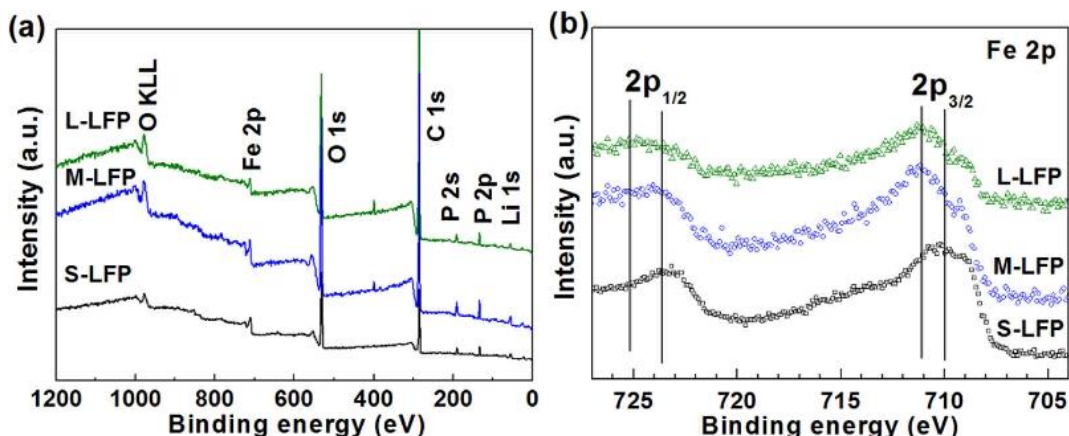
Figure 6. Survey XPS spectrum (a) and high-resolution Fe 2p spectrum (b) of the S-LFP sample.

XPS is a common method to obtain the chemical composition of elements and the valence state analysis of elements. Figure 6 shows the XPS plots of the S-LFP sample. In general, Fe $2p^{3/2}$ and Fe $2p^{1/2}$ bonds can occur at 710 and 724 eV, corresponding to Fe^{2+}, and at 712 and 726 eV, corresponding to Fe^{3+} [37]. Figure 6b shows that Fe $2p^{3/2}$ and Fe $2p^{1/2}$ of the L-LFP and M-LFP materials were shifted from 710 and 724 eV towards higher bond energies with increasing particle size of LFP materials, which could be due to the formation of the Fe(III) state in the LFP sample with a larger particle size.
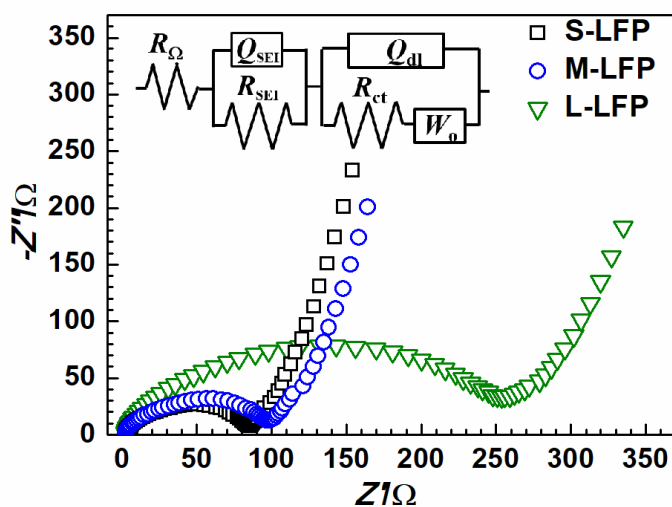
Figure 7. Electrochemical impedance spectroscopy (EIS) plots of the S-LFP, M-LFP and L-LFP samples.

To further analyse the effect of the particle size of $FePO_4 \cdot 2H_2O$ on the electrical properties of the LFP materials, electrochemical impedance spectroscopy (EIS) measurements of the samples were carried out in the discharge state, as shown in Figure 7. The EIS plot consists of a semicircle in the high or middle frequency range and an inclined line in the low frequency range. The semicircle and inclined line represent the charge transfer resistance (R_{ct}), Warburg resistance associated with the charge transfer resistance (R_{ct}) and Warburg resistance associated with the Li^+ diffusion coefficient (D_{Li}), respectively [38,39]. From Figure 7, it can be seen that S-LFP exhibits a smaller R_{ct} (84 Ω) than M-LFP (98 Ω) and L-LFP (248 Ω), indicating improved electronic conductivity for the S-LFP sample, which favoured its excellent electrochemical performance.

4. CONCLUSIONS

In summary, our results have shown that the particle size of $FePO_4 \cdot 2H_2O$ raw materials affected the particle size of LFP materials. The particle size of LFP materials is positively correlated with the particle size of $FePO_4 \cdot 2H_2O$ raw materials. The use of $FePO_4 \cdot 2H_2O$ raw materials with small particles contributes to the high purity and reduced particle size of LFP materials, thus leading to superior rate performance. The LFP materials prepared using small-sized $FePO_4 \cdot 2H_2O$ show high purity and small particle size, thus exhibiting an improved rate capacity and cycling stability. In addition, the LFP materials prepared using large-sized $FePO_4 \cdot 2H_2O$ exhibited a longer slope voltage at the end of the discharge curve, which may be due to no lithiation of the large-sized $FePO_4 \cdot 2H_2O$ core during the sintering process. Our research suggests that it is important to improve the electrochemical performance of LFP materials by controlling the particle size of $FePO_4 \cdot 2H_2O$ raw materials in the process of carbothermal reduction using $FePO_4 \cdot 2H_2O$ raw materials, which is an economical and efficient large-scale method.

References

1. J. Wang and X. Sun, *Energy Environ. Sci.*, 5 (2012) 5163.
2. J.B. Goodenough and K.S. Park, *J. Am. Chem. Soc.*, 135 (2013) 1167.
3. A.K. Padhi, K.S. Nanjundaswamy and J.B. Goodenough, *J. Electrochem. Soc.*, 144 (1997) 1188.
4. C. Masquelier and L. Croguennec, *Chem. Rev.*, 113 (2013) 6552.
5. N. Ravet, Y. Chouinard, J.F. Magnan, S. Besner, M. Gauthier and M. Armand, *J. Power Sources*, 97 (2001) 503.

6. Y. Zhou, C.D. Gu, J.P. Zhou, L.J. Cheng, W.L. Liu, Y.Q. Qiao, X.L. Wang and J.P. Tu, *Electrochim. Acta*, 56 (2011) 5054.
7. W. Sun, C. Deng, H. Hao, Y. Kang and Y. Si, *Mater. Lett.*, 93 (2013) 49.
8. R. Dominko, J.M. Goupil, M. Bele, M. Gaberscek, M. Remskar, D. Hanzel and J. Jamnik, *J. Electrochem. Soc.*, 152 (2005) A858.
9. H. Shu, X. Wang, W. Wen, Q. Liang, X. Yang, Q. Wei, B. Hu, L. Liu, X. Liu, Y. Song, M. Zhou, Y. Bai, L. Jiang, M. Chen, S. Yang, J. Tan, Y. Liao and H. Jiang, *Electrochim. Acta*, 89 (2013) 479.
10. H. Shu, X. Wang, Q. Wu, B. Hu, X. Yang, Q. Wei, Q. Liang, Y. Bai, M. Zhou, C. Wu, M. Chen, A. Wang and L. Jiang, *J. Power Sources*, 237 (2013) 149.
11. Z. Ma, G. Shao, G. Wang, Y. Zhang and J. Du, *J. Solid State Chem.*, 210 (2014) 232.
12. Z. Yang, J. Xia, L. Zhi, W. Zhang and B. Pei, *Ionics*, 20 (2014) 169.
13. M. Lin, Y. Chen, B. Chen, X. Wu, K. Kam, W. Lu, H.L.W. Chan and J. Yuan, *ACS Appl. Mater. Inter.*, 6 (2014) 17556.
14. C. Sun, S. Rajasekhara, J.B. Goodenough and F. Zhou, *J. Am. Chem. Soc.*, 133 (2011) 2132.
15. G. Xu, FengLi, Z. Tao, X. Wei, Y. Liu, X. Li, Z. Ren, G. Shen and G. Han, *J. Power Sources*, 246 (2014) 696.
16. C. Delacourt, P. Poizot, S. Levasseur and C. Masquelier, *Electrochem. Solid-State Lett.*, 9 (2006) A352.
17. M. Li, L. Sun, K. Sun, S. Yu, R. Wang and H. Xie, *J. Solid State Electrochem.*, 16 (2012) 3581.
18. Y. Wang and G. Cao, *Adv. Mater.*, 20 (2008) 2251.
19. H.K. Song, K.T. Lee, M.G. Kim, L.F. Nazar and J. Cho, *Adv. Funct. Mater.*, 20 (2010) 3818.
20. K.T. Lee and J. Cho, *Nano Today*, 6 (2011) 28.
21. Y. Zhao, L. Peng, B. Liu and G. Yu, *Nano Lett.*, 14 (2014) 2849.
22. G. Hu, X. Gao, Z. Peng, K. Du, X. Tan and Y. Liu, *Trans. Nonferrous Met. Soc. China*, 15 (2005) 795.
23. S.-Y. Chung, S.-Y. Choi, T. Yamamoto and Y. Ikuhara, *Angew. Chem. Int. Ed.*, 48 (2009) 543.
24. K. Hoang and M. Johannes, *Chem. Mater.*, 23 (2011) 3003.
25. J. Liu, R. Jiang, X. Wang, T. Huang and A. Yu, *J. Power Sources*, 194 (2009) 536.
26. P. Gibot, M. Casas-Cabanas, L. Lydia, L. Stephane, C. Philippe, H. Stéphane, J.-M. Tarascon and M. Christian, *Nat. Mater.*, 7 (2008) 741.
27. B. Kang and G. Ceder, *Nature*, 458 (2009) 190.
28. C. Delacourt, J. Rodríguez-Carvajal, B. Schmitt, J.-M. Tarascon and C. Masquelier, *Solid State Sci.*, 7 (2005) 1506.
29. P.S. Herle, B. Ellis, N. Coombs and L.F. Nazar, *Nat. Mater.*, 3 (2004) 147.
30. K. Zaghib, A. Mauger, F. Gendron and C.M. Julien, *Chem. Mater.*, 20 (2008) 462.
31. M. Wagemaker, D.P. Singh, W.J.H. Borghols, U. Lafont, L. Haverkate, V.K. Peterson and F.M. Mulder, *J. Am. Chem. Soc.*, 133 (2011) 10222.
32. P. Gąsiorski, M. Matusiewicz, E. Gondek, T. Uchacz, K. Wojtasik, A.Danel, Ya. Shchure and A.V. Kityk, *J. Lumin.*, 198 (2018) 370.
33. D.Yu. Gryzlov, S.A. Novikova, T.L. Kulova, A.M. Skundin and A.B. Yaroslavtsev, *Russ. J. Electrochem.*, 54 (2018) 442.
34. Y. Li, J. Hao, F. Wei, L. Fu, Y. Liu, Z. Wang, C. Yang and B. Li, *J. Mater. Sci. -Mater. Electron.*, 27 (2016) 9398.
35. L.-X. Yuan, Z.-H. Wang, W.-X. Zhang, X.-L. Hu, J.-T. Chen, Y.-H. Huang and J.B. Goodenough, *Energy Environ. Sci.*, 4 (2011) 269.
36. J. Yang, J. Wang, Y. Tang, D. Wang, X. Li, Y. Hu, R. Li, G. Liang, T.-K. Sham and X. Sun, *Energy Environ. Sci.*, 6 (2013) 1521.
37. L. Castro, R. Dedryvère, J.-B. Ledeuil, J. Bréger, C. Tessier and D. Gonbeau, *J. Electrochem. Soc.*, 159 (2012) A357.
38. Y. Li, Y. Zhang, J. Ma, L. Yang, X. Li, E. Zhao, S. Fan, G. Xu, S. Yang and C. Yang, *J.*

Int. J. Electrochem. Sci., 17 **(2022)** Article Number: 220722

11

Electrochem. Soc., 166 (2019) A410.
39. G. Hu, Y. Wang, K. Du, Z. Peng, X. Xie and Y. Cao, *J. Solid State Electrochem.*, 24 (2020) 2441.